Ann. Phys. (Berlin) 528, No. 7–8, 543–550 (2016) / DOI 10.1002/andp.201600014

annalen der physik

Bismuth telluride topological insulator nanosheet saturable absorbers for q-switched mode-locked Tm:ZBLAN waveguide lasers

Xiantao Jiang[1], Simon Gross[1], Han Zhang[2], Zhinan Guo[2], Michael J. Withford[1], and Alexander Fuerbach[1,]*

Received 18 January 2016, revised 27 March 2016, accepted 15 April 2016
Published online 2 May 2016

Nanosheets of bismuth telluride (Bi_2Te_3), a topological insulator material that exhibits broadband saturable absorption due to its non-trivial Dirac-cone like energy structure, are utilized to generate short pulses from Tm:ZBLAN waveguide lasers. By depositing multiple layers of a carefully prepared Bi_2Te_3 solution onto a glass substrate, the modulation depth and the saturation intensity of the fabricated devices can be controlled and optimized. This approach enables the realization of saturable absorbers that feature a modulation depth of 13% and a saturation intensity of 997 kW/cm^2. For the first time to our knowledge, Q-switched mode-locked operation of a linearly polarized mid-IR ZBLAN waveguide chip laser was realized in an extended cavity configuration using the topological insulator Bi_2Te_3. The maximum average output power of the laser is 16.3 mW and the Q-switched and mode-locked repetition rates are 44 kHz and 436 MHz, respectively.

1 Introduction

Mode-locked integrated mid-IR waveguide lasers with ultrashort pulse duration, high peak power, and high repetition rates are of great interest for a variety of applications like surgery, spectroscopy or pollution monitoring. In particular, the mid-IR water absorption peaks around 2 μm and 3 μm are extensively utilized in medical applications that require precise and minimally invasive procedures. In these cases the laser must induce a minimum of collateral thermal and photomechanical damage, which can be minimized by utilizing ultrashort laser pulses and by selecting specific laser wavelengths [1]. In addition, mode-locked lasers with ultrashort pulse duration and thus high peak power can be used for the generation of broadband emission in the mid-IR (2–10 μm) via supercontinuum generation [2]. As the vast majority of molecules exhibit highly specific absorption lines in this spectral “fingerprint” region, such lasers are ideal sources for applications such as pollution monitoring, LIDAR (Light Detecting and Ranging) as well as medical diagnostics [3–5].

Since waveguide lasers are embedded within a small block of gain material, they are inherently robust and immune to environmental fluctuations. Moreover, due to their small mode volumes, low lasing thresholds can be achieved. Thus, integrated waveguide chip laser architectures have been extensively studied in the past in rare-earth doped glasses [6, 7], ceramics [8, 9], and crystals [10, 11]. ZBLAN (ZrF_4-BaF_2-LaF_3-AlF_3-NaF) glass has been identified as an excellent host material for mid-infrared (mid-IR) application due to its excellent broadband transmission ranging from 250 nm to 7 μm as well as high solubility for rare-earth ions [12]. Up to date, high slope efficiency continuous wave (CW) lasers [7] as well as actively and passively Q-switched lasers [13, 14], operating at laser wavelengths ranging from 1 - 3 μm, have been successfully demonstrated by inscribing depressed cladding waveguides into rare-earth doped ZBLAN glass

* Corresponding author E-mail: alex.fuerbach@mq.edu.au
1 Centre for Ultrahigh bandwidth Devices for Optical Systems (CUDOS) and MQ Photonics Research Centre, Dept. of Physics and Astronomy, Macquarie University, NSW 2109, Australia
2 SZU-NUS Collaborative Innovation Centre for Optoelectronic Science and Technology, Key Laboratory of Optoelectronic Devices and Systems of Ministry of Education and Guangdong Province, College of Optoelectronic Engineering, Shenzhen University, Shenzhen, 518060, P.R. China

chips [15–17]. The potential for incorporating narrow-band Bragg-gratings as wavelength-selective elements into those chip lasers has also been investigated [18].

Passive mode-locking techniques have many advantages over active schemes that require active cavity length stabilization as well as bulky acousto-optic or electro-optic modulators. Up to now, passively mode-locked waveguide lasers have been demonstrated in rare-earth doped glasses and crystals using semiconductor saturable absorber mirrors (SESAMs) [19–22], carbon nanotubes [23, 24], and graphene [25–27] as saturable absorbers (SAs) in the near infrared (1 - 1.5 μm) range. Recently, Ren et al. reported Q-switched mode-locked operation of a waveguide laser at 2 μm wavelength using graphene [28].

In the last few years, topological insulators (TIs) have emerged as a promising candidate for broadband saturable absorbers. These topological insulators (TIs) exhibit surface/edge states that are metallic, strongly dispersive and cross the entire bulk insulating gap [29, 30]. Their Dirac cone-like electronic band structure is similar to that of graphene [31] and thus topological insulators exhibit broadband saturable absorption due to Pauli blocking under strong illumination. Bismuth telluride (Bi_2Te_3) has theoretically [32] and experimentally [33] been found to be a three-dimensional topological insulator material with a surface state that consists of a single nondegenerate Dirac-cone with a bulk energy gap of 0.17 eV [33, 34]. A single photon with a wavelength shorter than 7.5 μm (0.17 eV) can thus excite an electron from the valence band to the conduction band, while photons with wavelengths larger than 7.5 μm can excite one electron from the conduction band to surface/edge states. Interband scattering between excited bulk conduction band states and surface/edge states results in a quasi-equilibrium condition on a timescale of 500 fs [35]. This means that Bi_2Te_3 is an excellent candidate for use as a fast saturable absorber. Previously, passive mode-locking has been demonstrated in bulk and fiber lasers using Bi_2Te_3 [36–46], as well as its TI siblings Bi_2Se_3 [47, 48] and Sb_2Te_3 [49, 50] at various wavelengths ranging from the near to the mid-IR, by means of end facet coupling, perpendicular insertion into the laser resonator, or evanescent field interaction. However, mode-locked pulse generation using topological insulators in waveguide lasers has not been reported yet.

In this work, waveguides were inscribed into thulium-doped ZBLAN glass via the femtosecond laser direct-write technique [51] and Bi_2Te_3 samples with different concentrations were utilized as saturable absorbers in an external cavity. For the first time to our knowledge, Q-switched Mode-Locked (QML) operation of a mid-IR ZBLAN waveguide chip laser was demonstrated using topological insulators. The maximum average output power of the laser is 16.3 mW and the Q-switched and mode-locked repetition rates are 44 kHz and 436 MHz respectively. This highlights the potential of topological insulators as novel saturable absorber materials for fully integrated waveguide chip lasers.

2 Fabrication of waveguides and Bi_2Te_3 saturable absorbers

Depressed cladding waveguides [18] were inscribed into Tm:ZBLAN glass samples (with a doping concentration of 3mol.% TmF_3) by the femtosecond laser direct-write technique using an ultrafast Ti:sapphire oscillator (Femtolasers GmbH, FEMTOSOURCE XL 500, 5.1MHz, 550 nJ, 50 fs). Initiated by nonlinear absorption of the high-intensity femtosecond laser pulses, a larger fraction of single bridging fluorine bonds relative to double bridging bonds are formed during the laser inscription process compared to the pristine glass. This resulting in a local rarefaction and a negative refractive index change in the ZBLAN glass [52]. The resulting index change between core and cladding is -1×10^{-3} to -1.5×10^{-3} [7] and the core diameter and length of the waveguides used in our experiments are 50 μm and 12 mm, respectively. One end of the waveguide chip was cut at Brewster's angle to permit the set up of an external cavity.

Stoichiometric Bi_2Te_3 nanosheets were synthesized by the hydrothermal interaction/exfoliation approach [41]. The Bi_2Te_3 nanosheets were then dissolved in de-ionized water because isopropanol or acetone reacts with PVA resulting in PVA aggregation. The Bi_2Te_3 nanosheets were subsequently dissolved in de-ionized water with a concentration of 1 mg/ml and ultrasonicated for 2 hours. Solid white PVA was also dissolved in de-ionized water with a concentration of 100 mg/ml and water-bath heating for 2 hours at 100°C. The 1 mg/ml Bi_2Te_3 solution was then mixed with the 100 mg/ml PVA solution at a ratio of 2:1, and ultrasonicated for 2 hours to be used as a spin coating precursor. To obtain different Bi_2Te_3 concentrations on 170 μm thick UV fused silica glass substrates, multiple layers of solution were spin coated on the glass substrates, increasing from 5 to 15 layers, all with the same fabrication procedures: 400 rpm for 15 s, and 1200 rpm for 15 s, followed by heating for 30 s on an 80 °C clean thermostatic plate. Homogenous, precisely concentration controlled and repeatable Bi_2Te_3 SA samples could be prepared following this recipe.

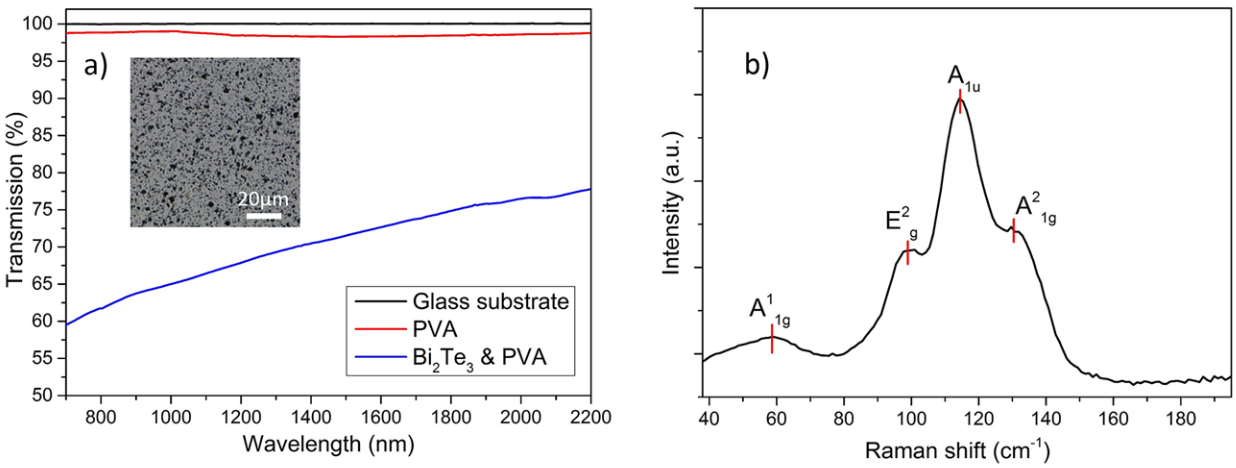

Figure 1 a) Absorption spectrum of pure PVA and of 15 layers of Bi_2Te_3 dissolved in PVA deposited on a 1 mm fused silica glass substrate (referenced to a clean glass substrate). The insert shows a brightfield image of a Bi_2Te_3 SA sample taken with an optical microscope (40x objective). b) Raman spectrum of Bi_2Te_3 nanosheets.

3 Characterization of the Bi_2Te_3 saturable absorbers

Figure 1a shows the linear absorption spectrum of pure PVA and Bi_2Te_3 with PVA (15 layers) deposited on a 1 mm fused silica glass substrate. An uncoated glass substrate was used as a reference to remove Fresnel reflections in our measurements. Pure PVA has a high transmission in the entire measurement range from 500 to 2000 nm in agreement with previous reports [46, 53]. Bi_2Te_3 also exhibits broadband transmission characteristic from 500 to 2000 nm (and beyond) due to its Dirac-cone like zero bandgap electronic energy structure. This makes Bi_2Te_3 a saturable absorber material suitable from the visible to the mid-IR wavelength range.

The nanosheet structure of Bi_2Te_3 has been confirmed by Raman spectroscopy using a 785 nm excitation laser (Figure 1b). The four measured Raman peaks are located at 58.8, 99.9, 114.2 and 130.8 cm^{-1} corresponding to the $A^1{}_{1g}$, $E^2{}_g$, A_{1u} and $A^2{}_{1g}$ peaks, respectively. Compared with bulk Bi_2Te_3 crystal, the appearance of the additional A_{1u} Raman mode is explained by the size of the Bi_2Te_3 particles decreasing to 200 - 300 nm, which breaks the crystalline symmetry of the bulk Bi_2Te_3 [38, 40]. The nonlinear optical transmission of the Bi_2Te_3 SA samples with different spin coating layers was characterized using an open aperture Z-scan setup [58, 61] with an acousto-optically (AO) Q-switched 1880 nm laser source. The Q-switching frequency varied from 20 kHz to 100 Hz, while the full width at half maximum (FWHM) of the Q-switched pulse varied from 550 to 200 ns. Using a 50 mm focusing lens, the maximum intensity on the SA was 100 MW/cm^2. The measured nonlinear transmission T was fitted based on a two-level saturable absorber model [62, 63] with an intensity dependent transmission according to

$$T(I) = \exp\left[-\left(\alpha_{NS} + \frac{\alpha_0}{1 + {}^{I}/_{I_A}}\right)\right], \tag{1}$$

where I_A is the saturation intensity, and α_{NS} and $\alpha_S = \frac{\alpha_0}{1+I/I_A}$ are the nonsaturable and saturable absorption components. The modulation depth of different Bi_2Te_3 samples measured in our experiments is defined as the normalized transmittance difference between high and low irradiation intensities according to

$$\Delta T = \frac{exp(-\alpha_{NS}) - exp[-(\alpha_{NS} + \alpha_0)]}{exp(-\alpha_{NS})} = 1 - exp(-\alpha_0)\,. \tag{2}$$

The measured saturation intensities and modulation depths for different absorbers are summarized in Figure 2. It can be seen that the saturation intensity and the modulation depth can be precisely controlled by changing the number of spin coated layers of Bi_2Te_3 solution and thus the concentration of Bi_2Te_3. It is important to note that modest modulation depths were achieved at saturation intensities more than one order of magnitude smaller than the previous reports as shown in Figure 3. This means that the concentration of Bi_2Te_3 in our samples is likely to be much lower compared to previous reports, yet our fabrication process ensures that our saturable absorbers still feature modulation depths of up to 13.2% which is very high compared to well-established

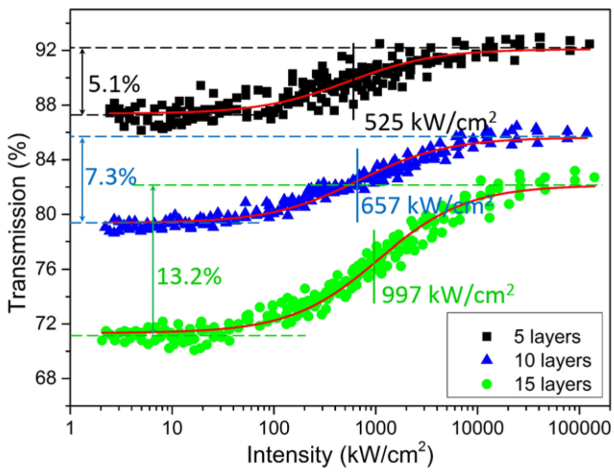

Figure 2 Measured nonlinear transmission characteristics of Bi_2Te_3 saturable absorbers with different number of coating layers at 1880 nm. The modulation depth and saturation intensities are labeled in the figure.

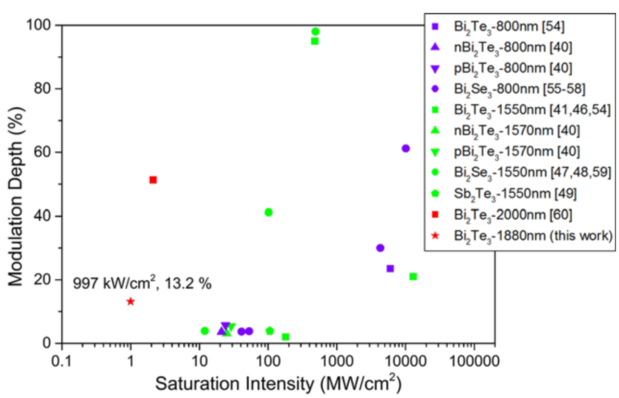

Figure 3 Overview of reported modulation depths and saturation intensities of saturable absorbers based on the topological insulator materials Bi_2Te_3, Bi_2Se_3 and Sb_2Te_3.

saturable absorbers like carbon nanotubes (CNTs, modulation depth: ~1% [64]). Since the intensity levels in integrated waveguide lasers are typically smaller than that of bulk or fiber lasers, it is important that a saturable absorber has both a high modulation depth and a low saturation intensity.

4 Laser performance and discussion

The saturation intensities and modulation depths of Bi_2Te_3 SAs reported in the literature vary widely and the vast majority of experiments have been carried out at 800 nm and 1550 nm, as illustrated in Figure 3. Thus, in order to study and optimize the properties of Bi_2Te_3

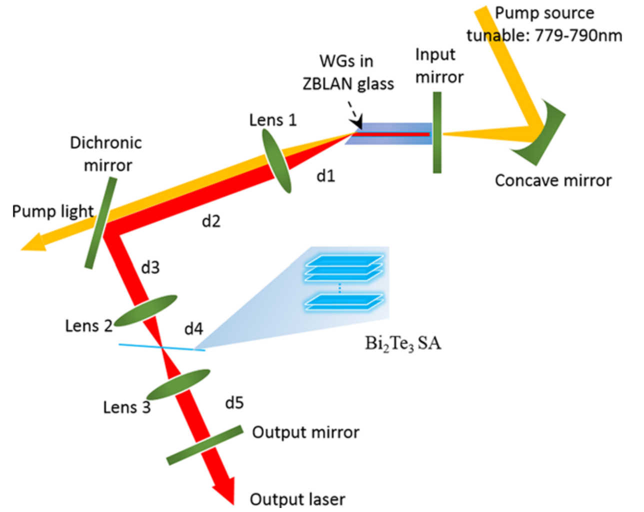

Figure 4 Schematic of the experimental setup. The waveguide chip is cut at Brewster's angle at one end. The waveguide diameter and length are 50 μm and 12 mm respectively. The focal length of lenses 1–3 are 40, 20 and 20 mm, respectively. The distances d1, d2, d3, d4 and d5 are 40, 145, 60, 40 and 35 mm, respectively. The pump source is a diode laser in Littrow configuration with a tunable wavelength from 779 to 790 nm.

saturable absorbers for mid-IR waveguide chip lasers, an external cavity was built as shown in Figure 4. This setup allows for comparing different samples in the same setup and to control and vary the spot size and thus irradiation intensity on the absorbers. It should be noted, that the optimised SA could eventually be directly coated onto a waveguide chip resulting in a monolithic laser. The pump source was a tapered external-cavity diode laser in Littrow configuration that enables the pump wavelength to be tuned from 779 to 790 nm in order to optimize the pump efficiency. The maximum available pump power was 1.7 W. One end facet of the WG chip was butt-coupled to a dichroic input coupling mirror, while the other facet was cut at Brewster angle to avoid Fresnel reflections and to achieve a linearly polarized laser output. Since the linear transmission spectrum of Bi_2Te_3 (see Figure 1a) reveals a non-negligible absorption at the pump wavelength, a dichroic mirror was used to avoid linear absorption of the pump light at the SA and thus thermally damage of the SA over time. Lens 2 was used to focus the laser beam onto the Bi_2Te_3 SA that was placed between lens 2 and 3 under Brewster's angle to avoid unwanted reflections and Fabry-Perot effects. A 91% reflective mirror was used as the output coupler. In an external cavity it is crucial to match the beam diameter of the resonator mode at the Brewster's cut chip end-facet to the diameter of the waveguide mode. The

Original Paper

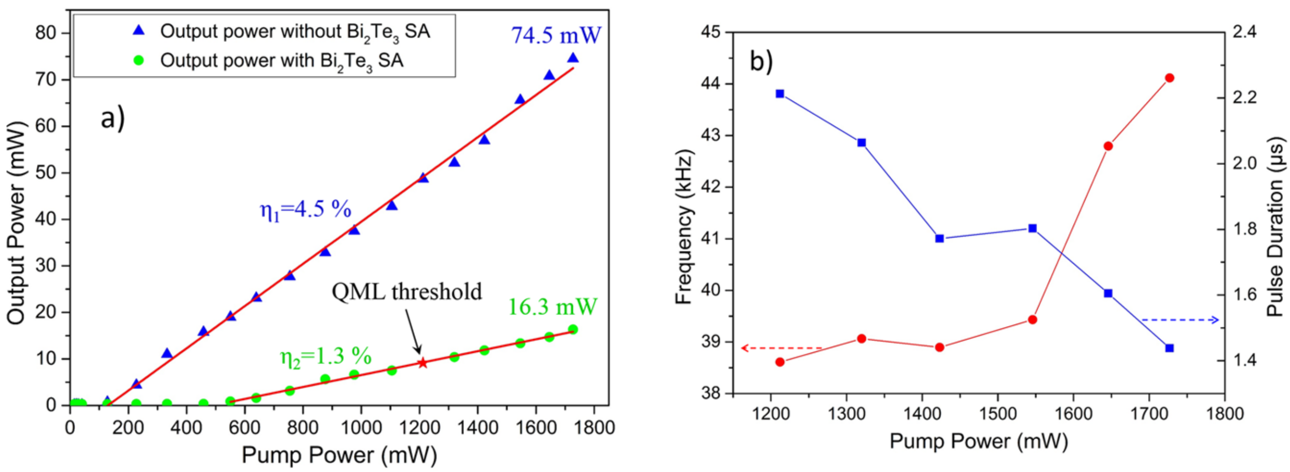

Figure 5 a) Laser characteristic for the resonator with and without saturable absorber inserted. The QML operation threshold is 1212 mW. b) Frequency and pulse duration of the Q-switched pulses as a function of pump power.

losses coming from mode-mismatch or unstable oscillation resulted in a lower slope efficiency compared with previous report [7], and >70 mW CW average output power can be delivered at full pump power as shown in Figure 5a.

Bi_2Te_3 samples with different coating layers were tested within the same optical resonator. Using Bi_2Te_3 SAs with 5 and 10 layers respectively, Q-switched mode-locked pulses could be observed at the output of the laser. However, the generated pulse trains exhibited large intensity fluctuations of about 20% and were only stable for a few minutes. The unstable QML operation is attributed to the too low saturation intensity and modulation depth of these two saturable absorbers. However, using the Bi_2Te_3 sample with 15 layers, highly stable Q-switched mode-locked laser pulses were successfully generated. The generated pulse train was highly stable with over a timescale of 60 minutes, and the output power has 0.8% fluctuation and 1.5% decrease, which are ascribed to the misalignment of the resonator and the thermal effects of the waveguide over time. The saturation intensity and modulation depth of this sample was 997 kW/cm^2 and 13.2%, respectively. Although a further increase in the concentration of Bi_2Te_3 would lead to an even higher modulation depth, it would also result in non-saturable losses in excess of 20%, resulting in an increased laser threshold and a decreased slope efficiency. As the generated pulse train with the 15 layer absorber was highly stable over a long period of time, we conclude that this is an appropriate concentration for our given laser geometry.

Using the 15 layer sample, the slope efficiency decreased from 4.5 % to 1.3% and the CW laser threshold increased from 66 mW to 527 mW, as shown in Figure 5a. When the pump power reached a value of 1212 mW, stable Q-switched mode-locked laser pulse could be observed. Purely Q-switched operation was not observed between CW and QML operation. A typical oscilloscope trace of the Q-switched model-locked laser output is shown in Figure 6. The observed peaks in the radio frequency (RF) spectrum at the mode-locking and Q-switching frequencies were 10 and 23 dB at the threshold pump power and increased to 22 and 27 dB at the maximum pump power as shown in Figure 6b and c. The Q-switching frequency increased from 38.6 to 44.1 kHz, while the full width half maximum pulse duration decreased from 2.2 to 1.4 μs as the pump power increased. The mode-locking frequency was consistent with the cavity length and was measured to be 436 MHz, independent on pump power. The maximum output power was 16.3 mW, which is higher than the recently reported average output power of a Q-switched mode-locked laser based on a short thulium-doped YAG waveguide and using a graphene saturable absorber [28].

The average output power at the QML threshold is 9.2 mW resulting in an average intra-cavity power of 102 mW. The calculated beam radii on the saturable absorber are 10 μm in the (y-z) plane and 12 μm in the (x-z) plane and thus the average intensity on the Bi_2Te_3 SA is 25.6 kW/cm^2 at the QML threshold. Note that this is still significantly lower than the measured saturation intensity of 997 kW/cm^2. However, the Q-switched mode-locked pulses grow from noise peaks near the threshold, and thus the actual peak intensity on the absorber approaches the saturation value at already relatively low average power levels.

For CW-mode locking to occur, the intra-cavity pulse energy must fulfill the condition [19]

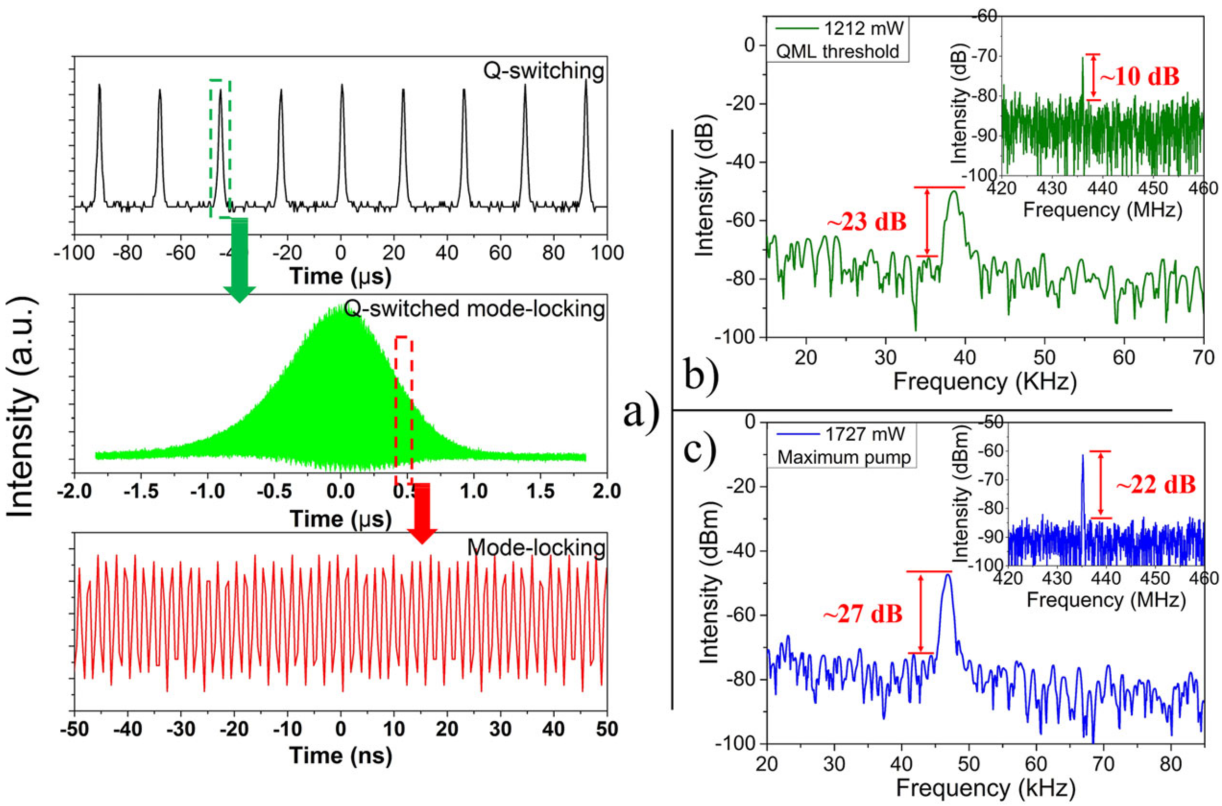

Figure 6 Q-switched mode-locked laser performance. *a) Oscilloscope traces of the Q-switched mode-locked pulse train, shown at different time resolutions. The top plot shows the train of the Q-switched pulse envelopes, the middle plot is a close-up view of a single Q-switched pulse, indicating the underlying mode-locked pulse train and the lower plot finally shows the mode-locked pulse train during a very short time-interval (100 ns) within a single Q-switched pulse*, b) and c) RF-spectrum of the laser output under QML operation exhibiting a peak at the Q-switched frequency of around 40 kHz and also at the mode-locked frequency of 436 MHz. The RF-spectrum is shown at the QML threshold (b) and at maximum pump power (c).

$$\left|\frac{dT}{dE_p}\right| E_p < r\frac{t_R}{\tau_L}, \quad (3)$$

where T is transmission of the saturable absorber, E_p is the incident pulse energy density,τ_L is the upper-state lifetime of the gain medium, t_R is the round-trip time and r is the pump parameter that indicates how many times the laser is pumped above threshold. Since the lifetime of the $^3F_4 \rightarrow {}^3H_6$ transition in Tm:ZBLAN glass is 11 ms long [65, 66], and the round-trip time of the external cavity is 2.26 ns short, it is challenging to achieve pure CW mode-locking. However, for many applications requiring high peak intensity (e.g. supercontinuum generation) QML can be an advantage as it can provide higher peak intensity-levels than pure CW mode-locking alone.

Due to the broad emission spectrum of Tm:ZBLAN, the optical spectrum of the QML laser has a 15 nm wide emission band ranging from 1865 to 1880 nm. The spectrum was stable during QML operation and is shown in Figure 7a. The output beam profile was elliptical due to the Brewster's angle of the waveguide chip, and had a beam diameter of 2.8 and 3.6 mm in the (y-z) and (x-z) plane, respectively, as shown in Figure 7b,. The diameter ratio at these two planes is 0.77, which agrees well with the calculated result of 0.74 (Figure 7c). It is also worth noting that the laser was oscillating in a purely fundamental transverse mode, even though the diameter of the waveguide was 50 μm. The large fundamental transverse mode is a direct result of the higher losses for higher-order transverse mode in the depressed index cladding geometry [7] and is important for avoiding optical damage and excessive nonlinear optical effects within a pulsed waveguide chip.

5 Summary

In conclusion, saturable absorbers based on nanosheets of the topological insulator material Bi_2Te_3 were fabricated using a multi-layer spin-coating technique. The

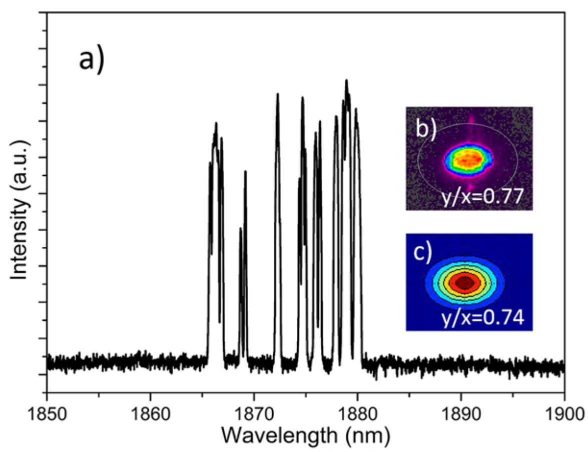

Figure 7 a) Optical spectrum of the QML laser. b) Measured output beam profile with an ellipticity of 0.77; c) Calculated beam profile of the laser output (ellipticity = 0.74).

saturation parameters of those saturable absorbers is proportional to the concentration of Bi_2Te_3 and can therefore be tailored by the number of coating layers. Due to Bi_2Te_3's Dirac-cone like energy structure, it features a broadband saturable absorption spectrum with an ultrafast relaxation time which makes it an excellent candidate for the Q-switched and mode-locked operation of chip lasers in the mid-IR. Using a saturable absorber with an optimized number of Bi_2Te_3 layers, for the first time to our knowledge, linearly polarized Q-switched mode-locking laser pulses have been realized from a Tm:ZBLAN waveguide chip laser in an extended cavity configuration. The observed Q-switching and mode-locking frequencies were 44 kHz and 436 MHz, respectively and the maximum output power was 16.3 mW.

Acknowledgements. This work was supported by the Australian Research Council Centres of Excellence scheme (project number CE110001018) and the National Natural Science Fund of China (grant number 61435010). S. Gross acknowledges funding from a Macquarie University Research Fellowship. X. Jiang acknowledges support from an iMQRES scholarship.

Key words. topological insulator, Bi_2Te_3, femtosecond laser direct-write, Tm:ZBLAN waveguide laser, Q-switched mode-locking.

References

[1] B. Jean and T. Bende, Solid-State Mid-Infrared Laser Sources, I. Sorokina, and K. Vodopyanov, eds. (Springer Berlin Heidelberg, 2003), pp. 530–565.

[2] A. V. Husakou and J. Herrmann, Phys. Rev. Lett. **87**, 203901 (2001).

[3] B. I. Vasil'ev and M. Oussama, Quantum Electron. **36**, 801 (2006).

[4] V. Kondepati, H. M. Heise, and J. Backhaus, Anal. Bioanal. Chem. **390**, 125–139 (2008).

[5] I. Melngailis, IEEE Trans. Geosci. Electron. **10**, 7–17 (1972).

[6] S. Taccheo, G. Della Valle, R. Osellame, G. Cerullo, N. Chiodo, P. Laporta, O. Svelto, A. Killi, U. Morgner, M. Lederer, and D. Kopf, Opt. Lett. **29**, 2626–2628 (2004).

[7] D. G. Lancaster, S. Gross, H. Ebendorff-Heidepriem, K. Kuan, T. M. Monro, M. Ams, A. Fuerbach, and M. J. Withford, Opt. Lett. **36**, 1587–1589 (2011).

[8] G. A. Torchia, A. Rodenas, A. Benayas, E. Cantelar, L. Roso, and D. Jaque, Appl. Phys. Lett. **92**, 111103 (2008).

[9] T. Calmano, A. G. Paschke, J. Siebenmorgen, S. T. Fredrich-Thornton, H. Yagi, K. Petermann, and G. Huber, Appl. Phys. B **103**, 1–4 (2011).

[10] T. Calmano, J. Siebenmorgen, O. Hellmig, K. Petermann, and G. Huber, Appl. Phys. B **100**, 131–135 (2010).

[11] Y. Tan, A. Rodenas, F. Chen, R. R. Thomson, A. K. Kar, D. Jaque, and Q. Lu, Opt. Express **18**, 24994–24999 (2010).

[12] J. M. Parker, Annu. Rev. Mater. Sci. **19**, 21–41 (1989).

[13] D. G. Lancaster, S. Gross, A. Fuerbach, H. E. Heidepriem, T. M. Monro, and M. J. Withford, Opt. Express **20**, 27503–27509 (2012).

[14] J. H. Lee, S. Gross, B. V. Cunning, C. Brown, D. Kielpinski, T. M. Monro, and D. G. Lancaster, *CLEO: 2014*(Optical Society of America, San Jose, California, 2014), p. JTu4A.128.

[15] G. Palmer, S. Gross, A. Fuerbach, D. G. Lancaster, and M. J. Withford, Opt. Express **21**, 17413–17420 (2013).

[16] D. G. Lancaster, S. Gross, H. Ebendorff-Heidepriem, A. Fuerbach, M. J. Withford, and T. M. Monro, Opt. Lett. **37**, 996–998 (2012).

[17] D. G. Lancaster, S. Gross, H. Ebendorff-Heidepriem, M. J. Withford, T. M. Monro, and S. D. Jackson, Opt. Lett. **38**, 2588–2591 (2013).

[18] S. Gross, M. Ams, D. G. Lancaster, T. M. Monro, A. Fuerbach, and M. J. Withford, Opt. Lett. **37**, 3999–4001 (2012).

[19] E. R. Thoen, D. J. Jones, F. X. Kartner, E. P. Ippen, and L. A. Kolodziejski, IEEE Photon. Technol. Lett., **12**, 149–151 (2000).

[20] J. B. Schlager, B. E. Callicoatt, R. P. Mirin, and N. A. Sanford, IEEE Photon. Technol. Lett. **14**, 1351–1353 (2002).

[21] A. Choudhary, A. A. Lagatsky, P. Kannan, W. Sibbett, C. T. A. Brown, and D. P. Shepherd, Opt. Lett. **37**, 4416–4418 (2012).

[22] A. A. Lagatsky, A. Choudhary, P. Kannan, D. P. Shepherd, W. Sibbett, and C. T. A. Brown, Opt. Express **21**, 19608–19614 (2013).

[23] G. Della Valle, R. Osellame, G. Galzerano, N. Chiodo, G. Cerullo, P. Laporta, O. Svelto, U. Morgner, A. G.

Rozhin, V. Scardaci, and A. C. Ferrari, Appl. Phys. Lett. **89**, 231115 (2006).
[24] S. J. Beecher, R. R. Thomson, N. D. Psaila, Z. Sun, T. Hasan, A. G. Rozhin, A. C. Ferrari, and A. K. Kar, Appl. Phys. Lett. **97**, 111114 (2010).
[25] R. Mary, G. Brown, S. J. Beecher, F. Torrisi, S. Milana, D. Popa, T. Hasan, Z. Sun, E. Lidorikis, S. Ohara, A. C. Ferrari, and A. K. Kar, Opt. Express **21**, 7943–7950 (2013).
[26] A. G. Okhrimchuk, and P. A. Obraztsov, Sci. Rep. **5**, 11172 (2015).
[27] A. Choudhary, S. Dhingra, B. D'Urso, P. Kannan, and D. P. Shepherd, IEEE Photon. Technol. Lett. **27**, 646–649 (2015).
[28] Y. Ren, G. Brown, R. Mary, G. Demetriou, D. Popa, F. Torrisi, A. C. Ferrari, F. Chen, and A. K. Kar, IEEE J. Sel. Top. Quantum Electron. **21**, 1602106 (2015).
[29] C. L. Kane, and E. J. Mele, Phys. Rev. Lett. **95**, 146802 (2005).
[30] L. Fu, C. L. Kane, and E. J. Mele, Phys. Rev. Lett. **98**, 106803 (2007).
[31] G.-K. Lim, Z.-L. Chen, J. Clark, R. G. S. Goh, W.-H. Ng, H.-W. Tan, R. H. Friend, P. K. H. Ho, and L.-L. Chua, Nat. Photon. **5**, 554–560 (2011).
[32] H. J. Zhang, C. X. Liu, X. L. Qi, X. Dai, Z. Fang, and S. C. Zhang, Nat. Phys. **5**, 438–442 (2009).
[33] Y. L. Chen, J. G. Analytis, J.-H. Chu, Z. K. Liu, S.-K. Mo, X. L. Qi, H. J. Zhang, D. H. Lu, X. Dai, Z. Fang, S. C. Zhang, I. R. Fisher, Z. Hussain, and Z.-X. Shen, Science **325**, 178–181 (2009).
[34] G. A. Thomas, D. H. Rapkine, R. B. Van Dover, L. F. Mattheiss, W. A. Sunder, L. F. Schneemeyer, and J. V. Waszczak, Phys. Rev. B **46**, 1553–1556 (1992).
[35] M. Hajlaoui, E. Papalazarou, J. Mauchain, G. Lantz, N. Moisan, D. Boschetto, Z. Jiang, I. Miotkowski, Y. P. Chen, A. Taleb-Ibrahimi, L. Perfetti, and M. Marsi, Nano Lett. **12**, 3532–3536 (2012).
[36] Z.-C. Luo, M. Liu, H. Liu, X.-W. Zheng, A.-P. Luo, C.-J. Zhao, H. Zhang, S.-C. Wen, and W.-C. Xu, Opt. Lett. **38**, 5212–5215 (2013).
[37] P. X. Li, G. J. Zhang, H. Zhang, C. J. Zhao, J. J. Chi, Z. Q. Zhao, C. Yang, H. W. Hu, and Y. F. Yao, IEEE Photon. Technol. Lett. **26**, 1912–1915 (2014).
[38] C. Cheolhwan, L. Junsu, K. Joonhoi, and L. Ju Han, Laser Phys. **24**, 105106 (2014).
[39] M. Jung, J. Lee, J. Koo, J. Park, Y.-W. Song, K. Lee, S. Lee, and J. H. Lee, Opt. Express **22**, 7865–7874 (2014).
[40] Y.-H. Lin, S.-F. Lin, Y.-C. Chi, C.-L. Wu, C.-H. Cheng, W.-H. Tseng, J.-H. He, C.-I. Wu, C.-K. Lee, and G.-R. Lin, ACS Photon. **2**, 481–490 (2015).
[41] C. Zhao, H. Zhang, X. Qi, Y. Chen, Z. Wang, S. Wen, and D. Tang, Appl. Phys. Lett. **101**, 211106 (2012).
[42] K. Yin, B. Zhang, L. Li, T. Jiang, X. Zhou, and J. Hou, Photon. Res. **3**, 72–76 (2015).
[43] T. J. Ke Yin, Xin Zheng, Hao Yu, Xiangai Cheng, and Jing Hou, arXiv:1505.06322 (2015).
[44] J. Lee, J. Koo, Y. M. Jhon, and J. H. Lee, Opt. Express **22**, 6165–6173 (2014).
[45] H. Mu, Z. Wang, J. Yuan, S. Xiao, C. Chen, Y. Chen, Y. Chen, J. Song, Y. Wang, Y. Xue, H. Zhang, and Q. Bao, ACS Photon. **2**, 832–841 (2015).
[46] D. Mao, B. Jiang, X. Gan, C. Ma, Y. Chen, C. Zhao, H. Zhang, J. Zheng, and J. Zhao, Photon. Res. **3**, A43–A46 (2015).
[47] C. Zhao, Y. Zou, Y. Chen, Z. Wang, S. Lu, H. Zhang, S. Wen, and D. Tang, Opt. Express **20**, 27888–27895 (2012).
[48] H. Liu, X.-W. Zheng, M. Liu, N. Zhao, A.-P. Luo, Z.-C. Luo, W.-C. Xu, H. Zhang, C.-J. Zhao, and S.-C. Wen, Opt. Express **22**, 6868–6873 (2014).
[49] J. Boguslawski, J. Sotor, G. Sobon, J. Tarka, J. Jagiello, W. Macherzynski, L. Lipinska, and K M. Abramski, Laser Phys. **24**, 105111 (2014).
[50] J. Sotor, G. Sobon, W. Macherzynski, P. Paletko, K. Grodecki, and K. M. Abramski, Opt. Mater. Express **4**, 1–6 (2014).
[51] R. R. Gattass, and E. Mazur, Nat. Photon. **2**, 219–225 (2008).
[52] S. Gross, D. G. Lancaster, H. Ebendorff-Heidepriem, T. M. Monro, A. Fuerbach, and M. J. Withford, Opt. Mater. Express **3**, 574–583 (2013).
[53] G. Attia, and M. F. H. Abd El-kader, Int. J. Electrochem. Sci. **8**, 5672–5687 (2013).
[54] S. Chen, C. Zhao, Y. Li, H. Huang, S. Lu, H. Zhang, and S. Wen, Opt. Mater. Express **4**, 587–596 (2014).
[55] S. Lu, C. Zhao, Y. Zou, S. Chen, Y. Chen, Y. Li, H. Zhang, S. Wen, and D. Tang, Opt. Express **21**, 2072–2082 (2013).
[56] J. Du, Q. Wang, G. Jiang, C. Xu, C. Zhao, Y. Xiang, Y. Chen, S. Wen, and H. Zhang, Sci. Rep. **4**, 6346 (2014).
[57] Z. Luo, Y. Huang, J. Weng, H. Cheng, Z. Lin, B. Xu, Z. Cai, and H. Xu, Opt. Express **21**, 29516–29522 (2013).
[58] L. Zhengqian, L. Chun, H. Yizhong, W. Duanduan, W. Jianyu, X. Huiying, C. Zhiping, L. Zhiqin, S. Liping, and W. Jian, IEEE J. Sel. Top. Quantum Electron. **20**, 1–8 (2014).
[59] Y. Chen, C. Zhao, H. Huang, S. Chen, P. Tang, Z. Wang, S. Lu, H. Zhang, S. Wen, and D. Tang, J. Lightwave Technol. **31**, 2857–2863 (2013).
[60] J. Li, H. Luo, L. Wang, C. Zhao, H. Zhang, H. Li, and Y. Liu, Opt. Lett. **40**, 3659–3662 (2015).
[61] M. Sheik-Bahae, A. A. Said, T. H. Wei, D. J. Hagan, and E. W. Van Stryland, IEEE Quantum Electron. **26**, 760–769 (1990).
[62] Q. Bao, H. Zhang, Y. Wang, Z. Ni, Y. Yan, Z. X. Shen, K. P. Loh, and D. Y. Tang, Adv. Funct. Mater. **19**, 3077–3083 (2009).
[63] S. Wang, H. Yu, H. Zhang, A. Wang, M. Zhao, Y. Chen, L. Mei, and J. Wang, Adv. Mater. **26**, 3538–3544 (2014).
[64] Y. Jong Hyuk, C. Won Bae, S. Lee, Y. H. Ahn, K. Kihong, L. Hanjo, G. Steinmeyer, V. Petrov, U. Griebner, and F. Rotermund, Appl. Phys. Lett. **93**, 161106 (2008).
[65] J. L. Doualan, S. Girard, H. Haquin, J. L. Adam, and J. Montagne, Opt. Mater. **24**, 563–574 (2003).
[66] B. M. Walsh, and N. P. Barnes, Appl. Phys. B **78**, 325–333 (2004).